ARMA 16-803

Active ultrasonic imaging and interfacial characterization of stationary and evolving fractures in rock

Pourahmadian, F. and Guzina, B.B.

Department of Civil, Environmental, and Geo- Engineering, University of Minnesota, Minneapolis, MN, USA

ABSTRACT: The objective of this study is to deploy ultrasonic waves toward better understanding of preexisting and evolving fractures in rock, with the dual focus on i) reconstructing the curvilinear fracture geometry, and ii) mapping the distribution of its heterogeneous specific (shear and normal) stiffness. This is accomplished via the 3D Scanning Laser Doppler Vibrometer (SLDV) that is capable of monitoring the triaxial particle velocity at every scan point on the sample's surface. Experiments are performed on slab-like granite specimens featuring either stationary or evolving fractures where the fracturing, in the latter case, occurs in 3-point bending configuration. The rock specimens are then excited, under the plane stress condition, by a piezoelectric transducer at 20-30kHz, while the in-plane velocity response of the sample is monitored over a rectangular region covering the fracture. Thus obtained full-field data are next used to recover both the fracture geometry, and to expose its nonlinear contact behavior. The latter is then approximated point-wise in terms of the linearized contact properties i.e. specific (shear and normal) stiffness, whose recovered spatial variations for stationary and advancing fractures are found to conform with expected trends.

1. INTRODUCTION

Geometric and interfacial properties of fractures and related features (e.g. faults) in rock and other like materials are the subject of critical importance to a wide spectrum of scientific and technological facets of our society including energy production from natural gas and geothermal resources (Baird et al. 2013, Verdon and Wustefeld 2013, Taron and Elsworth 2010), seismology (McLaskey et al. 2012), hydrogeology (Cook 1992), environmental protection (Place et al. 2014), and mining (Gu et al. 1993). Unfortunately, a direct access to fracture surfaces in rock is, in most field situations, either non-existent or extremely limited (e.g. via isolated boreholes, shafts, or adits), which necessitate the use of remote sensing techniques where the contact law at the boundary of rock discontinuities is often assumed to be linear and represented in a *parametric* fashion via e.g. the so-called (shear and normal) *specific stiffness,* relating the contact traction to the jump in displacements across the interface (Schoenberg 1980). Despite its heuristic and simplistic nature, the fracture's interfacial stiffness matrix not only is proven to be immediately relevant to the stress and thus stability analyses in rock masses (Eberhardt et al. 2004), but also bears an intimate connection to the fracture's hydraulic properties (Pyrak-Nolte and Nolte 2016, Pyrak-Nolte and Morris 2000), and may serve as a precursor of progressive shear failure along rock discontinuities (Hedayat et al 2014).

In this spirit, the aim of this work is to: 1) *non-parametrically* expose the true contact law and its spatiotemporal variations along the surface of stationary and propagating fractures in rock, and 2) extract the *linearized* contact properties in terms of the shear and normal specific stiffness — together with their heterogeneous distribution along the fracture. This is accomplished in a laboratory setting by monitoring the full-field interaction of ultrasonic shear waves (propagating through granite specimens) with stationary and advancing fractures via a recently acquired 3D Scanning Laser Doppler Vibrometer (SLDV) that is capable of monitoring triaxial particle velocity, with frequencies up to 1MHz, over the surface of rock specimens with 0.1mm spatial resolution and O(nm) displacement accuracy. Looking forward, the full-field seismic observations such as those presented herein may not only help decipher the true physics of a fracture interface and shine light on fidelity of classical interface models, but may also provide the ground truth toward validating the next generation of seismic imaging tools for simultaneous reconstruction and interfacial characterization of fractures in rock from *remote* sensory data (Pourahmadian and Guzina 2015).

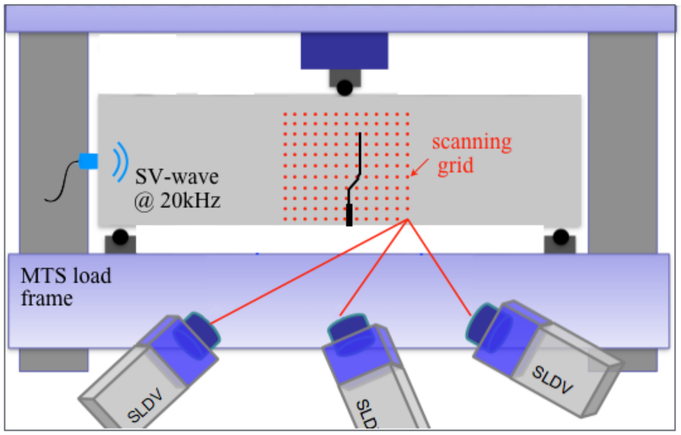

Fig. 1. Schematic of the SLDV sensing configuration for imaging and characterization of an evolving fracture.

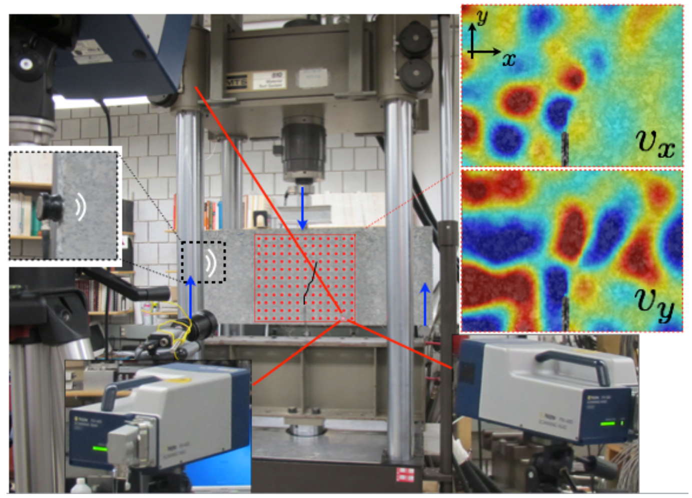

Fig. 2. Full-field ultrasonic sensing of an advancing fracture: the specimen is fractured in the 3-point bending configuration; at a fixed CMOD, ultrasonic waves are induced in the sample while the surface particle velocities (in the x- and y-directions) are measured over the scanning grid via SLDV.

2. EXPERIMENTAL SETUP

Experiments are performed on two slab-like prismatic specimens of *charcoal* and *Rockville granite* with dimensions 0.96m × 0.3m × 0.03m, designed such that: a) the largest specimen dimension is almost one meter in order to enable the *propagation* of low-frequency (i.e. long-wavelength) waves through the sample; and b) the 0.03m slab thickness is at least decade-smaller than the remaining characteristic dimensions of the problem in order to approximate the *plane-stress* condition at lower excitation frequencies, where the shear-wavelength-to-slab-thickness ratio is $\lambda_S/h > 5$. Note that in this frequency range, the phase error committed by the *plane stress* approximation is less than 3% (Tokmashev et al. 2013). Under such conditions, the SLDV-captured surface motion can be taken as being uniform *throughout* the thickness of a granite slab. For further reference, the nominal material properties of the featured rock types are listed in Table 1 (Zietlow and Labuz 1998).

Table 1. Nominal properties of the featured rock materials

Rock	E [GPa]	ν	ρ [Kg/m^3]	c_p [m/s]	c_s [m/s]
Rockville	25	0.2	2720	3196	1955
charcoal	70	0.24	2800	5428	3175

With reference to Fig. 1, the geometric reconstruction and interfacial characterization of an *evolving fracture* is pursued by fracturing a Rockville-granite slab in a three-point bending (3PB) configuration and sensing the fracture surface periodically during the loading process. This is accomplished by (i) generating the shear waves by an ultrasonic transducer, emitting a modulated five-cycle burst with the center frequency of 20kHz, and (ii) scanning the induced wave motion over the surface of a granite slab via SLDV. The tests were performed in the 1000kN MTS load frame (see Fig. 2), which has one meter clearance between columns, providing an unimpeded SLDV vantage of the specimen. In this approach, the crack initiation and propagation is controlled by a closed-loop, servo-hydraulic system with the crack mouth opening displacement (CMOD) as the feedback signal. Note that the 3PB testing with an eccentric notch gives rise to a *mixed-mode* loading, resulting in fracture propagation along a *curved* path. The target SLDV scan is performed at approximately 70% of the maximum load (post-peak regime) while keeping the CMOD *constant*.

For the experimental study of stationary fractures, a *through-fracture is* induced in the charcoal-granite slab via 3PB in an MTS load frame; the pieces are then reconnected by applying a very small normal load

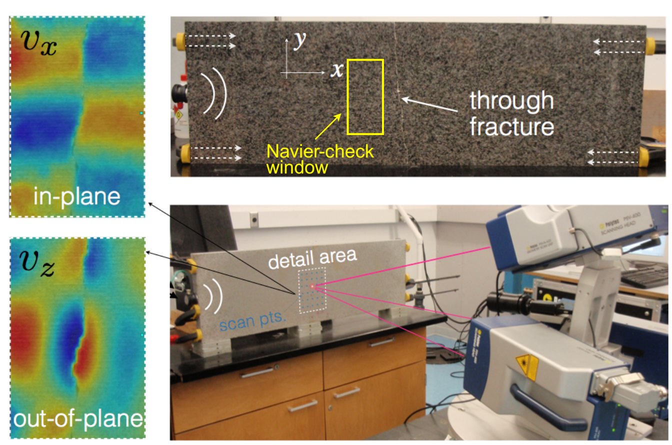

Fig. 3. fractured granite slab (top right), SLDV testing configuration (bottom right), and snapshot in time of the particle velocity field across the fracture (left). The experimental wavefield is constructed via a rectangular grid of 37×48 scan points with the mean spacing of 4 mm.

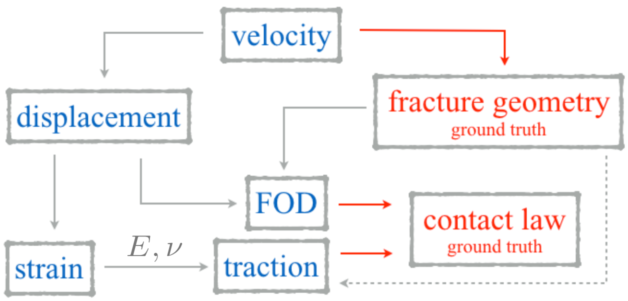

Fig. 4. Roadmap for the geometric reconstruction and non-parametric interfacial characterization of fractures from full-field SLDV data.

(O(10kPa)) to the opposite sides of the specimen using clamps, see Fig. 3. As in the case of an advancing fracture, the sample was excited by elastic shear waves at 20kHz, while monitoring the full-field surface motion is via SLDV. For further reference, it is noted that the dominant shear wave length, at 20kHz, in the charcoal (resp. Rockville) granite is λ_S~*16*cm (resp. λ_S~10cm).

3. RESULTS AND DISCUSSION

With reference to Fig. 4, the SLDV-measured velocity fields in the neighborhood of a fracture are processed to recover the fracture's geometry and interfacial behavior as described in the sequel. ***Geometric reconstruction***. It is apparent from Fig. 2 and Fig. 3 that the interaction of ultrasonic shear waves with a fracture gives rise to *discontinuity* in the wavefield across the interface. Thus, to obtain the fracture geometry, one may (at every snapshot in time) compute the jump in both (v_x and v_y) velocity distributions in the *x*- and *y*-directions. Then, by integrating the absolute value of thus obtained jump fields over the entire time span, one finds the plots as in Fig. 5 over the scanned area where the points of highest cumulative jump expose the fracture's true geometry. ***Contact law***. The idea behind *non-parametric* identification of the fracture's contact behavior is to extract i) the profile of fracture opening displacement (FOD), and ii) the distribution of tractions along the fracture from particle-velocity measurements on both sides of the discontinuity. Then, by plotting in time the (shear and normal) traction versus affiliated FOD – for every point along the fracture edge, one may retrieve the "true" spatiotemporal variation of the interfacial behavior. ***Signal Processing***. *A* suitable band-pass filter, with cut-off frequencies of 10kHz and 30kHz (catering for the spectrum of the source wavelet), is applied to the raw particle velocity signals measured at *every* scan point. Thus obtained smooth velocity signals are then numerically integrated, and high-pass filtered to eliminate the low-frequency drift due to integration. In this way, one obtains the "raw" displacement fields

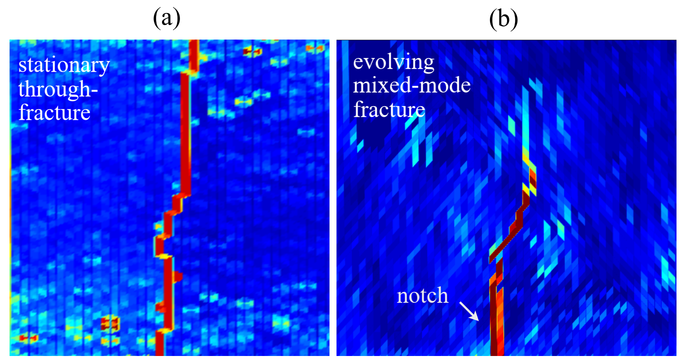

Fig. 5. Reconstructed fracture geometries from SLDV wavefields measured over 0.4m × 0.3m windows around the fractures: a) stationary fracture in charcoal granite, and b) advancing fracture in Rockville granite at 70% post-peak load.

shown in the left panel of Fig. 6, which are smooth and differentiable in time, yet *non-smooth in space*. However, with reference to Fig. 4, these fields must provide the basis for the computation of strain and stress fields in the rock slab. To resolve the problem, a two-step spatial smoothing is applied to such "raw" displacements at every snapshot in time. First, a median-based moving average filter (with the spatial extent of $\lambda_S/8$) is applied to eliminate bad scan points i.e. sudden spikes in the data, and to stabilize the next (interpolation) step. Second, the resulting displacement distributions are then approximated by *double Fourier series* (including up to seven harmonics) in *x*- and *y*-directions. This gives birth to the smooth displacement fields shown in the right panel of Fig. 6, which are now differentiable both in

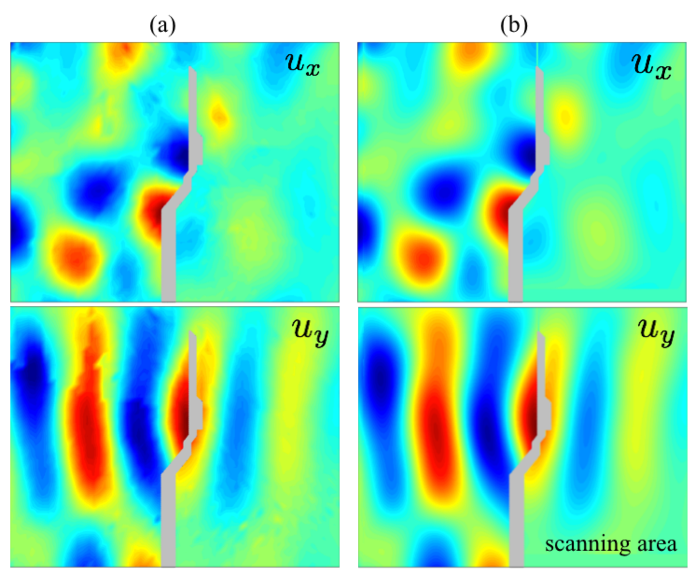

Fig. 6. Displacement fields in x- and y-directions at one snapshot in time (over a 0.4m×0.3m window around the advancing fracture at 70% post-peak): a) raw waveforms, and b) smooth fields obtained after signal processing.

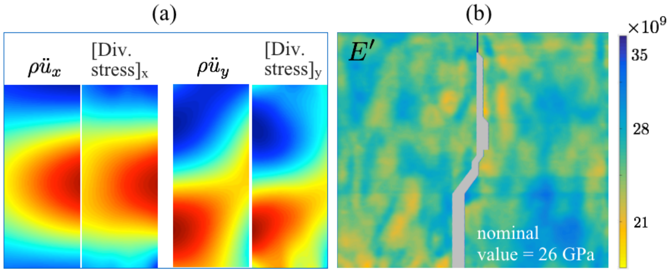

Fig. 7. a) SLDV-observed balance (along x and y directions) in the plane-stress Navier equation in a 0.05m × 0.15m window located near the stationary fracture (see the top-right panel in Fig. 3), and b) recovered distribution of the Young's modulus over the scanning area using elastography.

time and space, and can thus be used to compute the strain components as needed. Given the (previously recovered) fracture geometry, one may further compute the FOD profile along the fracture mid-section by *extending* the smooth displacement fields from both sides to this line, see Fig. 6(b).

For the purpose of calculating the stress fields from the available strain distributions, one needs to implement the Hooke's law which requires knowledge of the specimens' elastic moduli. While the nominal values of the latter are reported in Table 1, one may alternatively take advantage of the *full-field* SLDV data to recover the (generally heterogeneous) distribution of the Young's modulus and Poisson's ratio over the scanned area, which carries the potential of furnishing a more robust stress estimation. ***Elastography***. This concept was first introduced in the context of biomedical imaging (Ophir et al. 1999), and the core idea, adapted for the purpose of this study, is as follows: given smooth and differentiable displacement fields u_x and u_y over the scanning region (see Fig. 6(b)) during certain time interval, the distribution of elastic moduli in this area may be obtained by pointwise solving the 2D Navier equation in terms of the sought-for material properties. More specifically, the Navier equation is recast, under the plane stress assumption, as

$$\begin{bmatrix} \ddot{u}_x & \left(\frac{1}{2}(u_{x,yy}+u_{y,xy})-u_{y,yx}\right) \\ \ddot{u}_y & \left(\frac{1}{2}(u_{y,xx}+u_{x,yx})-u_{x,xy}\right) \end{bmatrix} \begin{bmatrix} \frac{\rho}{E'} \\ \nu \end{bmatrix} = \begin{bmatrix} \left(\frac{1}{2}(u_{x,yy}+u_{y,xy})+u_{x,xx}\right) \\ \left(\frac{1}{2}(u_{y,xx}+u_{x,yx})+u_{y,yy}\right) \end{bmatrix} \qquad (1)$$

where $E' = E/(1-\nu^2)$ is the plane-stress Young's modulus, and over-dots indicate temporal differentiation. Note that the implicit postulate in (1) is that both Young's modulus and Poisson's ratio are assumed to be *locally constant*. Otherwise, (1) takes a much more complex form that also includes the spatial derivatives of the elastic parameters (Barbone and Gokhale 2004). In this setting, one may first assess the validity of the plane-stress assumption by substituting the *nominal* elastic parameters from Table 1 into (1), and visually comparing the left-hand side (divergence of the stress tensor) and the right-hand side (mass density times the acceleration vector) in the Navier equation. One example of such verification is shown in Fig. 7 (a), which shows a reasonable agreement between the two sides of the Navier equation. Next, returning to the principle of elastography, one may solve (1) *for the elastic parameters* at every scan point and average the resulting field over the entire time interval to obtain their spatial distribution, see Fig. 7(b) for an example of his recovered distribution of the Young's modulus. With such result in place, one may now compute the stress fields, and consequently the distribution of tractions along the fractures mid-section.

At this point, the true contact behavior at every point along the fracture may be exposed by plotting the shear and normal traction versus respective FOD over a given time interval T_i, i=1,2,… (whose duration is comparable to the dominant period of ultrasonic excitation), see Fig. 8. Phenomenologically, the traction – FOD plots in shear

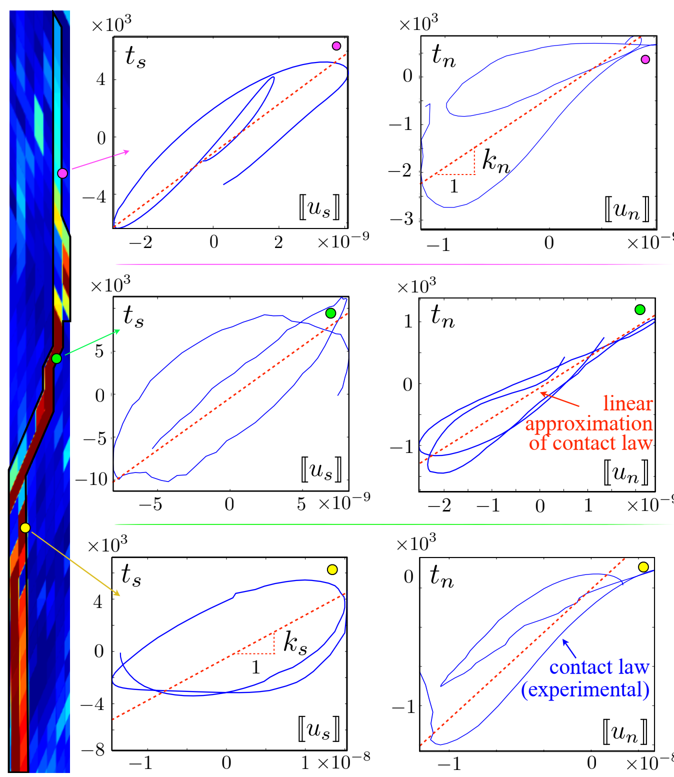

Fig. 8. The non-parametrically identified interfacial behavior in shear (t_s *vs* $[\![u_s]\!]$) and normal (t_n *vs* $[\![u_n]\!]$) directions at three points along the mixed-mode fracture (at 70% post-peak).

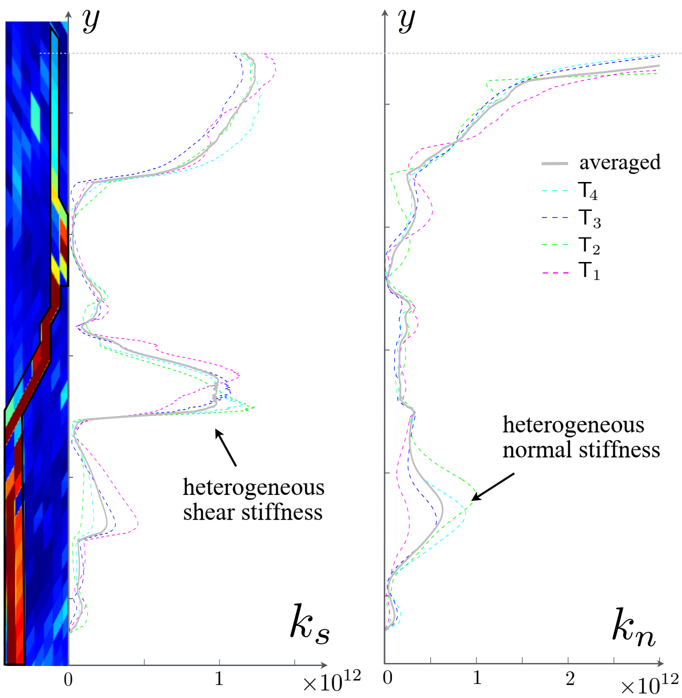

Fig. 9. Heterogeneous distribution of normal and shear specific stiffness along the boundary of a mixed-mode evolving fracture in Rockville granite (70% post-peak load), as recovered from the analysis of transient waveforms during 5 different time subintervals (T_i, i=1,2...5). Note that the vertical extent of the fracture (including the notch) is 25cm, which is approximately $2.5\lambda_s$ at 20kHz.

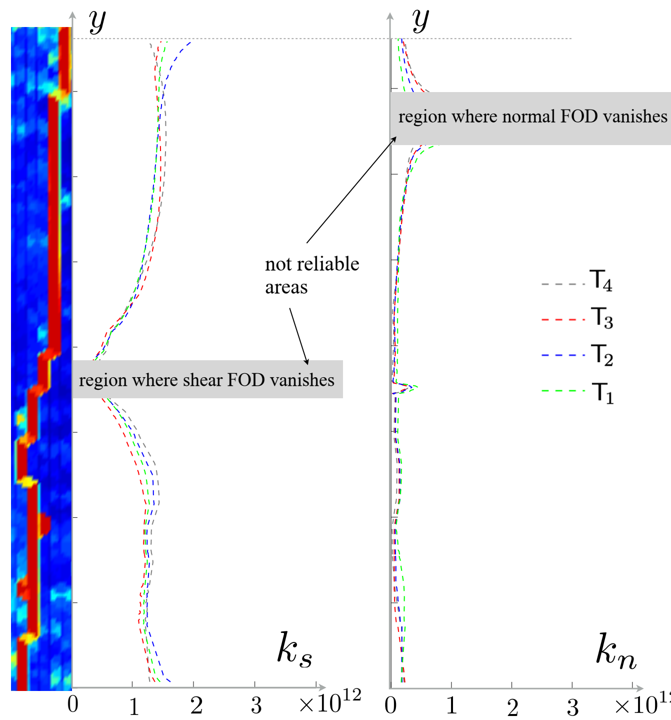

Fig. 10. Heterogeneous distribution of normal and shear specific stiffness along the boundary of a stationary through fracture in charcoal granite, as recovered from the analysis of transient waveforms during 5 different time subintervals (T_i, i=1,2...5). Note that the through fracture is subjected to a very small (O(10kPa)) normal stress, and that the vertical extent of the fracture (including the notch) is 30cm, which is approximately $2\lambda_s$ at 20kHz.

direction resembles the frictional hysteresis loops obtained by Ahmadian et al. 2010, and Pourahmadian et al. 2012. However, one should bear in mind that in this study the illuminating wavelet is *transient* — and thus it possesses a much wider frequency spectrum than the conventional steady-state and single-frequency excitations that are typically used for the dynamic analysis of frictional interfaces. Hence, one may not assume equivalence between the results of Fig. 8 – involving transient and multi-scale dynamics – with that of a steady-state behavior. On the other hand, the traction-FOD plots in normal direction feature a distinct cusp as FOD increases. This phenomenon may be affiliated with the well-known bi-linear behavior of frictional contacts in the normal direction (e.g. Jalali et al. 2011).

At a given time window T_i, one may replace the complex and nonlinear behavior of the interface with a *linearized behavior* by computing the average slope of the traction-FOD diagrams in the normal and shear directions to attain the so-called (normal and shear) *specific stiffness* respectively, given by the slopes of the dotted lines in Fig 8. Recovering these values for every point along the fracture, one arrives at the *heterogeneous distribution of interfacial stiffness* in shear and normal directions, as shown in Figs. 9 and 10 for the respective cases of propagating and stationary fractures. As expected, both normal an shear specific stiffness generally increase toward fracture tip in the case of an advancing fracture, while the stationary fracture is characterized by a rather uniform distribution of the pair of specific stiffnesses.

5. SUMMARY

This paper describes an initial study on the full-field ultrasonic investigation of stationary and advancing fractures in rock, effected via a 3D Scanning Laser Doppler Vibrometer (SLDV). The experiments are performed on slab-like specimens, allowing approximation of the underpinning wave propagation problem in terms of the plane-stress assumption. With suitable smoothing of the observed waveforms, it is shown that the proposed experimental procedure carries the potential of both i) reconstructing the curvilinear fracture geometry, and ii) point-wise identifying its true contact behavior, which can then be approximated in terms of customary linearized parameters of shear and normal specific stiffness.

ACKNOWLEDGEMENTS

The support provided by the National Science Foundation via Grant #1536110 and the University of Minnesota Supercomputing institute is kindly acknowledged.

REFERENCES

1. Ahmadian, H., H. Jalali, and F. Pourahmadian. 2010. Nonlinear model identification of a frictional contact support. *Mech. Syst. Signal Pr.* 24: 2844-2854.

2. Baird, A.F., J.M. Kendall, J.P. Verdon, A.Wuestefeld, T.E. Noble, Y. Li, M. Dutko, and Q.J. Fisher. 2013. Monitoring increases in fracture connectivity during hydraulic stimulations from temporal variations in shear wave splitting polarization. *Geophys. J. Int.*

3. Barbone, P.E., N.H. Gokhale. 2004. Elastic modulus imaging: on the uniqueness and nonuniqueness of the elastography inverse problem in two dimensions. *Inverse Problems*. 20: 283.

4. Cook, N.G.W. 1992. Natural joints in rock: Mechanical, hydraulic and seismic behaviour and properties under normal stress. *Int. J. Rock Mech. Min. Sci.* 29: 198-223.

5. Eberhardt, E., D. Stead, and J.S. Coggan. 2004. Numerical analysis of initiation and progressive failure in natural rock slopes – the 1991 Randa rockslide. *Int. J. Rock Mech. Min. Sci.* 41: 69-87.

6. Gu, W.H., N.R. Morgenstern, and P.K. Robertson. 1993. Progressive failure of lower San Fernando dam. *J. Geotech. Eng.* 119: 333-349.

7. Hedayat, A., L.J. Pyrak-Nolte, and A. Bobet. 2014. Precursors to the shear failure of rock discontinuities. *Geophys. Res. Lett.* 41: 5467-5475.

8. Jalali, H., H. Ahmadian, and F. Pourahmadian. 2011. Identification of micro-vibro-impacts at the boundary condition of a nonlinear beam. *Mech. Syst. Signal Pr.* 25: 1073-1085.

9. Knight, R., L.J. Pyrak-Nolte, L. Slater, E. Atekwana, A. Endres, J. Geller, D. Lesmes, S. Nakagawa, A. Revil, M. M. Sharma, and C. Straley. 2010. Geophysics at the interface: response of geophysical properties to solid-fluid, fluid-fluid, and solid-solid interfaces. *Reviews Geophysics*. 48.

10. McLaskey, G.C., A.M. Thomas, S.D. Glaser, and R.M. Nadeau. 2012. Fault healing promotes high-frequency earthquakes in laboratory experiments and on natural faults. *Nature.* 491: 101-104.

11. Ophir, J., S.K. Alam, B. Garra, F. Kallel, E. Konofagou, T. Krouskop, T. Varghese. 1999. *Proc. Inst. Mech. Eng. H J. Eng.* 213: 203-233.

12. Place, J., O. Blake, D. Faulkner, and A. Rietbrock. 2014. Wet fault or dry fault? A laboratory approach to remotely monitor the hydro-mechanical state of a discontinuity using controlled-source seismics. *Pure Appl. Geophysics*.

13. Pourahmadian, F., and B.B. Guzina. 2015. On the elastic-wave imaging and characterization of fractures with specific stiffness. *Int. J. Solids Struct*. 71: 126-140.

14. Pourahmadian, F., H. Ahmadian, and H. Jalali. 2012. Modeling and identification of frictional forces at a contact interface experiencing micro-vibro-impacts. *J. Sound Vib.* 331: 2874-2886.

15. Pyrak-Nolte, L.J., and D.D. Nolte. 2016. Approaching a universal scaling relationship between fracture stiffness and fluid flow. *Nat. Commun.* 7: 10663.

16. Pyrak-Nolte, L.J. and J.P. Morris. 2000. Single fractures under normal stress: The relation between fracture specific stiffness and fluid flow. *Int. J. Rock Mech. Min. Sci.* 37: 245-262.

17. Schoenberg, M. 1980. Elastic wave behavior across linear slip interfaces. *J. Acoust. Soc. Am.* 68: 1516-1521.

18. Taron, J. and D. Elsworth. 2010. Coupled mechanical and chemical processes in engineered geothermal reservoirs with dynamic permeability. *Int. J. Rock Mech. Min. Sci.* 47: 1339-1348.

19. Tokmashev, R.D., A. Tixier, and B.B. Guzina. 2013. Experimental validation of the topological sensitivity approach to elastic-wave imaging. *Inverse Problems.* 29: 125005.

20. Verdon, J.P. and A.Wustefeld. 2013. Measurement of the normal/tangential fracture compliance ratio (z_N/z_T) during hydraulic fracture stimulation using S-wave splitting data. *Geophys. Prospecting.* 61: 461-475.

21. Zietlow, W.K. and Labuz, J.F. (1998). Measurement of the intrinsic process zone in rock using acoustic emission. *Int. J. Rock Mech. Min. Sci.* 35: 291-299.